Enhanced Power Capability of Generator Units for Increased Operational Security using NMPC

Thomas Øyvang, *Member, IEEE,* Jonas Kristiansen Nøland, *Member, IEEE,* Roshan Sharma, Gunne J Hegglid, *Member, IEEE,* and Bernt Lie, *Member, IEEE*

***Abstract*—The ever-increasing penetration of intermittent energy sources introduces new demanding operating regimes for the bulk power generation in the power grid. During a worst-case power system disturbance scenario, the generator needs to operate beyond its limits to maintain stable operation. Therefore, a new online low-order thermal model of a hydrogenerator has been recently proposed, where the periodic extension of the long-forgotten capability diagram of the machine was in-depth investigated. An increased performance can be obtained if the total thermal capacity of the generator is exploited by applying optimal control theory in the Automatic Voltage Regulator (AVR). This paper proposes a Non-linear Model Predictive Controller (NMPC) combined with an Unscented Kalman Filter (UKF) with a modeling framework geared for use in a supervisory control structure for the conventional control system. The method provides maximum utilization of the machine's thermal capacity by providing the controller with an Enhanced Capability Diagram (ECD). Case studies on a single-machine system and a 16-bus multi-machine system were investigated. The results show that a satisfying controller action during different long-term voltage instability scenarios is realized.**

***Keywords*—Computerized monitoring and control, long-term voltage stability, non-linear model predictive control, supervisory control structure, thermal modeling, unscented kalman filter.**

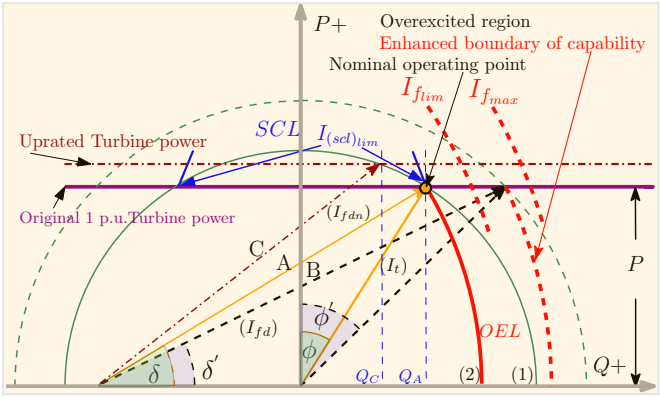

Fig. 1. Illustration of rated (A), enhanced (B), and uprated power (C) operating mode of a synchronous generator through an increased field current I_{fd} (2), and with the corresponding stator current I_t (1). Benchmark OELs consists of both a ceiling limit of the field current I_{fmax} (immediately response to overload), and a rotor load limit I_{flim} (with a delayed response). The dashed angle values (e.g., $\delta^{'}$) denote the extreme overexcited (enhanced) mode. The field current variation affects both the rotor angle (δ) and the power angle (ϕ).

I. Introduction

FUTURE operating regimes for conventional generators will demand higher operational flexibility due to an increase in the utilization of intermittent renewable energy (RE) [1]. Available system reserves must be utilized to preserve a robust power system security [2] from the synchronous generators. In a worst-case scenario, major catastrophic failures in large interconnected power systems [3] may lead to a blackout of the power system. Inadequate reactive power reserve affects the system reliability [4] and is one of the main reasons for a blackout [5] as it decreases the flexibility of the voltage control. There exists reactive power compensation equipment on the grid side. However, the most substantial portion of reactive power reserves relies on the capability of the large synchronous generators.

In a long-term voltage instability situation, the available voltage control capability of the power grid depends on the temperature rise of the synchronous generators [6]. In fact, the thermal overload capacity of the conventional power generation surpasses the virtual synchronous generators based on the Voltage Source Converter (VSC) technologies [7], [8]. The 'real' synchronous machines do not depend on the limitations in overload capability of power electronic components. Therefore, enhancing their reactive power margins is essential [9].

The periodic extension of the synchronous generator capability diagram has been largely overlooked. However, this trend is changing [10]. The temperature of the field winding and the overall MVA output (stator current) of the generator, determine the physical limitation of the reactive reserve power in the overexcited region. The generators in power systems are protected or controlled locally by devices such as the Over Excitation Limiter (OEL), and the Stator Current Limiter (SCL) as indicated in Fig. 1. Moreover, if the turbine power is increased (C in Fig. 1), the reactive power support of the machine may be further constrained (e.g., Q_C is more restrictive than the field heating Q_A). Extensive work has been carried out on the impact of OELs [11] and SCL [12]. In addition, a new approach was described for accurately determining the activation time of the protection system based on the available thermal capacity of the rotor [13]. However, all of those previous efforts were based on the principle of rigid pre-defined limitations. Hence, model-based online monitoring

The authors are with the Department of Electrical engineering, Information Technology and Cybernetics, University of South-Eastern Norway, Campus Porsgrunn, N-3918 Norway (e-mail: thomas.oyvang@usn.no; roshan.sharma@usn.no; gunne.j.hegglid@usn.no; bernt.lie@usn.no).

J.K. Nøland is with the Department of Electric Power Engineering, Norwegian University of Science and Technology, Norway (e-mail: jonas.k.noland@ntnu.no).

technologies have a huge potential for improving the control scheme and the utilization of the synchronous generator.

In particular, the model-predictive control (MPC) schemes have shown significant advantages for online voltage collapse prevention [14]. However, the focus has been on load tap control and thermal overloads of transmission lines [15], distributed MPC strategies [16], corrective control algorithms [17], and less attention towards the generation side. Recently, an active thermal management scheme based on the MPC concept of an Interior Permanent Magnet Synchronous Machine (IPMSM) has recently been proposed for lower temperature stress and longer lifetime [18]. However, this approach is not applicable for grid applications. Theoretically, MPC outperforms many other high efficient strategies [19] as it predicts the future behaviour of the plant with an internal prediction model. As the power system has a highly non-linear nature, e.g., time-varying setpoints, machine saturation, and possibly a subjected to large disturbances, more dedicated research towards Non-linear Model Predictive Control (NMPC) is necessary [20]. NMPC rises opportunities to implement fully non-linear models with non-linear constraints [21].

The estimator for the NMPC must be reliable and efficient. There are different alternatives for online state estimation, including Unscented Kalman Filter (UKF) [22], constrained UKF [23], extended particle filter (PF) [24], or observability of states of synchronous generators [25]. UKF is a modern algorithm (early 1990s) and is a well established robust filter algorithm [26]. As evident, UKF has some advantages for non-linear systems [27].

Recently, a low-order hybrid thermal-electrical model has been validated for a synchronous generator [28]. A significant improvement of the conventional controller may be achieved if an updated Enhanced Capability Diagram (ECD) is available for more advanced controllers in industrial applications [28]. This enhanced operating mode is schematically visualized in Fig. 1 (A and B).

A. Contributions and Outline of Paper

This paper presents a new NMPC supervisory control strategy of an advanced voltage control scheme for maximum utilization of a hydrogenerator in the overexcited region, employing the proposed ECD [28]. The control system combines a thermal-electrical model with a non-linear output feedback model predictive control (NMPC) and with Unscented Kalman Filtering (UKF). Both activation time and maximum values for OEL and SCL limiters are fully replaced by this control structure. However, the Under Excitation Limiter (UEL) is not considered as the enhanced under-excited mode is not relevant during a blackout (i.e., beyond the scope of the paper).

The paper is organized as follows. Section II describes the method used and the control structure formulation. Next, Section III presents an evaluation of the proposed control system on a single-machine case study. Section IV extends this case study for a multi-machine case system. Finally, Section V presents the discussion. Conclusions and future perspectives are presented in Section VI.

II. Developed Control Method

A. Overview

The online supervisory voltage control system proposed in this work is visualized in Fig. 2. This scheme can be further subdivided into a software and hardware part (frame). The software frame consist of an NMPC with an integrated thermal and electrical model, augmented UKF, and offline data for software setup and initialization of the models. The analytic thermal model must be calibrated to a Heat Run Test (HRT) [28] of the machine, and an initial value of the equivalent external reactance x_e is provided through a Short Circuit Analysis (SCA) offline. Data from the machine, excitation system, and AVR needs to be provided offline to setup the dynamic model. In addition, a limited finite element analysis (FEM) of each hydrogenerator for model fitting is beneficial [28]. Electrical quantities such as the active power P_t, the reactive power Q_t, the terminal current I_t, and the terminal voltage V_t are measured online from the generator terminals and are taken as outputs from the model. The amount of injected or absorbed reactive power given by the field current and the external grid, are strongly connected to the terminal voltage of the machine. The set-point (reference) of the AVR and the governor is provided in all simulations and available for the proposed control system. Additional outputs are temperatures measured from the stator copper T_s, the stator core T_{Fe}, and the air-to-water heat exchanger (e.g, warm air, T_{1i}). For increased robustness, phasor measurement units (PMUs) which are normally placed at sensitive locations throughout the transmission grid [29], can be utilized for estimating the external voltage level V_e. Both the field current I_{fd}, and the field voltage E_{fd} are used to estimate the rotor winding resistance R_r, and the rotor temperature T_r. A total of nine measurements ($m = 9$) are provided from the hydrogenerator as

$$y = [P_t, Q_t, E_{fd}, I_{fd}, V_t, I_t, T_s, T_{Fe}, T_{1i}]^T \tag{1}$$

The supervisory system is working as a master controller to the conventional AVR (primary). This is due to the fast excitation response time required in the system during transient disturbances. The objective of the proposed system is to work as a supervisory control for the machine based on the slow temperature dynamics in the machine. The control input, u_k, from the NMPC is a signal to the generator excitation system and governor system, and is implemented as a summation type, or take-over type control [11] in the conventional excitation system, and a reference step adjustment in the mechanical power P_{m0} as visualized in Fig. 2. Thus NMPC can work either as MISO (excitation control) or a MIMO system (excitation and turbine power). Moreover, the master controller is implemented with a DeadBand (DB) on the control inputs and activates if the field current is greater than a threshold value. When activated, it monitors temperatures on the conventional system and takes action through control inputs if necessary. Under normal conditions, the master controller is de-activated. It implies that both the field current and the temperatures in the controller horizon are below safe values.

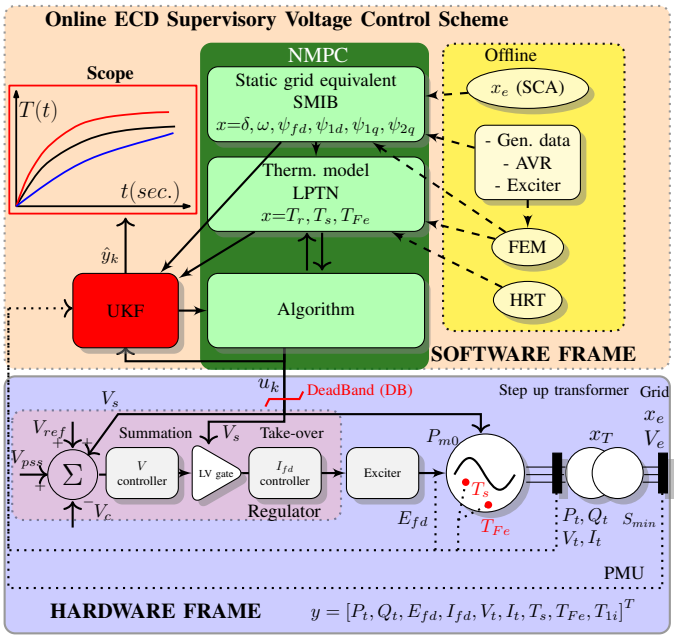

Fig. 2. Schematic diagram of the online ECD supervisory voltage control scheme. The hardware frame represents the actual aggregate connected to the grid carried out either as a single-machine system (e.g., as in Fig. 4) or as a 16-bus multi-machine system (e.g., as in Fig. 6). The online measurements y are indicated with dotted lines.

B. The prediction model

The internal NMPC prediction model consists of a low order thermal model [28] combined with an electrical model. The electrical model is a single machine infinite bus model (SMIB) where the hydrogenerator is modeled as a salient pole 2.1 model [30] (e.g., salient pole rotor structure means that ψ_{2q} in Eq. 5 is neglected). The field current of the machine I_{fd}, terminal current I_{t}, speed of the machine ω, and terminal voltage V_{t} are inputs to the thermal model. There are three coupled ODEs that govern the temperature distribution in the rotor copper T_r, the stator copper T_s, and the stator iron T_{Fe}:

$$\frac{dT_{\mathrm{r}}}{dt} = \frac{1}{\tau_{T,r}}\left[\frac{\Delta P_{\mathrm{r}}}{hA_{\mathrm{r}}} - (T_{\mathrm{r}} - T_{1,\mathrm{o}})\right] \tag{2}$$

$$\frac{dT_{\mathrm{s}}}{dt} = \frac{1}{\tau_{T,s}}\left[\frac{\Delta P_{\mathrm{s}}}{hA_{\mathrm{s}}} - (T_{\mathrm{s}} - T_{\mathrm{Fe}})\right] \tag{3}$$

$$\frac{dT_{\mathrm{Fe}}}{dt} = \frac{1}{\tau_{\mathrm{T,Fe}}}\left[\frac{\Delta P_{\mathrm{Fe}}}{hA_{\mathrm{Fe}}} + \frac{hA_{\mathrm{s}}}{hA_{\mathrm{Fe}}}(T_{\mathrm{s}} - T_{\mathrm{Fe}}) - (T_{\mathrm{Fe}} - T_{\delta})\right] \tag{4}$$

where A is the heat transfer surface in m^2, and h is the heat transfer coefficient in W/m^2K. The heat transfer hA in Eq.2 to Eq.4, are estimated from the heat-run test of the machine at stationary conditions and nominal values [28]. T_δ is the preheated air temperature in the air-gap, and $T_{1,o}$ is the cold cooling air. In addition, the different τ_T are the thermal time constants of the copper and the iron of the machine respectively [28]. The generator operates in a wide range of ambient temperatures as the cold-water temperature varies during the year. The cold-water temperature is the reference temperature of the system. There are nine states $(n = 9)$ in the prediction model in total,

$$x = [\delta, \omega, \psi_{fd}, \psi_{1d}, \psi_{1q}, \psi_{2q}, T_s, T_{Fe}, T_r]^T \tag{5}$$

where δ is the rotor angle, and ψ are the flux linkage states in the machine [30].

C. Identification of the external grid system

A static electric equivalent model is provided to represent the external grid system. Estimation of the static net equivalent consist of identifying the external reactance x_e (with resistance neglected), and the external voltage V_e. These variables are not simultaneously observable since they are coupled (x_e is given by the V_e/I relationship). Due to this, x_e is estimated initially offline through stationary short-circuit analysis (SCA), while the external voltage is estimated online. During a transmission system relay planning, the calculation of both maximum S_{max} and minimum S_{min} short-circuit power MVA (or impedance) for rated data of the electrical equipment and the topological arrangement of the system are done according to IEC 60909. S_{c_g} is the short circuit power of the generator. SCA analysis has the advantage of being possible both for existing systems and for systems at the planning stage. For convenience, the expected minimum MVA value S_{min} is used as the initial value for the external reactance x_e and is calculated from Eq.6. Grid faults may change the external reactance, and external voltage needs to be corrected through online PMU measurements.

$$x_e = \frac{V_e^2}{(S_{min}) - (S_{c_g})} \tag{6}$$

D. NMPC problem formulation and augmented UKF

The NMPC algorithm needs to know all system states x_k in real time. In practice, only certain measured outputs y_k are available. As a result, it cannot be expected that all the states are known or measured. To get around this problem, we estimate the states $\hat{x}_k$ using a state estimator and use the estimates of the states in the NMPC algorithm. The system states and the input disturbances estimated by the UKF, are fed as input to the NMPC. The overall control structure is schematically shown in Fig. 3.

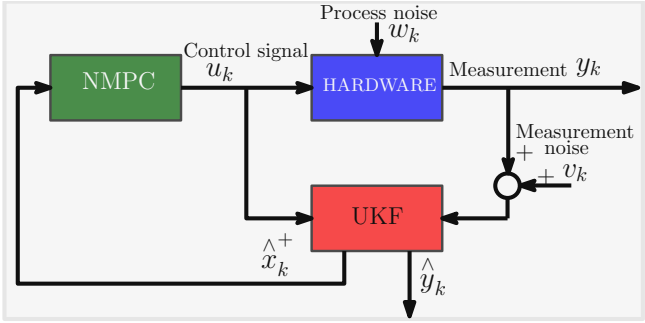

Fig. 3. Output feedback NMPC structure. This control structure is the basis for the ECD supervisory control shown in Fig. 2

Let the control deviation vector e be

$$e_j = \left[V_{ref,j} - V_{t,j}, P_{m_{ref,j}} - P_{e,j}\right] \tag{7}$$

Likewise, let the control vector u be

$$u_j = [V_{s,j}, P_{m0,j}]. \tag{8}$$

The model is now

$$x_{j+1} = f\left(x_j, u_j\right) \tag{9}$$

A standard quadratic performance index J is used to define the objective function of the NMPC problem formulation,

$$\min \quad J = \sum_{j=1}^{N_p} e_j^T \mathbf{Q} e_j + \sum_{j=1}^{N_c} \Delta u_{j-1}^T \mathbf{R} \Delta u_{j-1} \tag{10}$$

where

$$\Delta u_j = u_j - u_{j-1} \tag{11}$$

and matrices $\mathbf{Q}$ and $\mathbf{R}$ are positive definite and often chosen to be diagonal. N_p and N_c are prediction and control horizon lengths. The optimal control solution is found by minimizing the performance index J w.r.t. u, by Eqs. 7 - 11, and with given constraints. The solution gives optimal inputs $u_j^*, j \in \{0, N_c - 1\}$ in the NMPC. Only the first control input in the sequence of future inputs is actually used at each time-step, e.g., set $u_0 = u_0^*$, and the whole process of forming an optimal control problem and then solving it, is repeated. Because of the non-linear model in Eqs. 9, there is no guarantee of finding the global minimum. By here, it is assumed that the traditional controller gives a decent solution for normal operation. The suggested control input from the traditional controller is used as an initial guess in the optimization algorithm, and the subsequent optimizations are warm-started from the previous optimal solution. Due to the slow temperature dynamics of the system, the sample time Δt is in the range of 1 sec. to 1 min. In addition, the prediction horizon length should cover the open-loop transient system response and are determined to be $N_p = 10$, while the control horizon are $N_c = 2$. The weighting factors in eq. (10) are appropriately tuned for an optimal response (to avoid temperature overshoots) of the supervisory controller in MIMO mode for the case considered. In fact, the turbine power reduction should stabilize the critical temperature of the response for an extended under-voltage ride-through time (should not be over-weighted). In addition, it should contribute when the excitation power is constrained to ramp down (causing a potential loss of synchronism). Moreover, in MISO mode, there are only contributions from the voltage part of eq. (10).

The control inputs should lie between a minimum and a maximum value. These have been implemented as inequality constraints. In addition, to ensure that the maximum permitted temperature rise from the design specifications (e.g. insulation class F) is not violated, constraints are implemented for stator copper T_s, and rotor copper T_r.

The augmented UKF algorithm [27] can be used to estimate both the unmeasured states and unmeasured disturbances. The estimates of measured outputs typically constitute filtering of the measurements. Process w_k and measurement v_k noise are assumed to be known and implemented as Gaussian white noises. The input disturbance V_e is assumed to be slowly varying or constant and driven by white noise and has to be augmented with the input disturbance model.

With states and input disturbance estimated via the UKF algorithm, the NMPC is equipped with the necessary information to enable computation of future control inputs that will give optimal performance [27].

III. Single Machine Case Study

This section evaluates the single machine performance of the proposed ECD control system in comparison to a benchmark OEL system and an improved thermal-based system [13]. All systems include short-term capabilities. In fact, the OEL systems employ a combination of the instantaneous and the inverse-time pickup characteristics. The setting of the instantaneous limiter is about 1.6 times the rated field current. Alternatively, [13] and [31] uses the thermal inertia of the machine for identifying the activation time of the OEL. For performance comparison with the benchmark method, the thermal-based method presented in [13] is also implemented.

The single-machine test system is presented in Fig. 4, which is adapted from [13]. The hydrogenerator under consideration is the test machine from [28]. Considering the proposed system, it is equipped with a supervisory system as a MISO controller for OEL testing. In the proposed method, the single-machine test system monitors the temperature of the rotor T_r and ensures that it is protected against maximum overheating. The system also includes a pre-specified margin of 15 K identified from FEM analysis (temperature between hot-spot and observable temperature). From [6], it is intended that the temperature should not exceed 155 ^{o}C for class (F) insulation systems. A continuous time benchmark OEL introduced by PSAT is used in this model setup. In addition, a typical under-load tap changing (ULTC) continuous time transformer model is implemented at the load site. The simulations in this case study are performed using OpenIPSL in Dymola in combination with a Functional Mockup Unit (FMU) in Simulink. It is the maximum allowable field current from the various systems that are of interest. To compare temperatures, the ramp down of the benchmark OEL is not initiated. The start time for ramping down the excitation current from the improved OEL and proposed ECD systems is indicated in Fig. 5. The necessary OEL system parameters of the test machine for the improved OEL approach is presented in Table I. The comparison considers a tripping event (t = 1s) in one of the transmission lines between Bus 1 and 3. The response of the different excitation control methods (with summation type control) are presented and compared in Fig. 5. Finally, the comparative analysis is presented in Table II.

As indicated in Table II, the proposed ECD system yields an excellent improvement in the short-term reactive power capacity and further extends the capability of the improved OEL method [13]. This is achieved by a flexible ramp down time (limited by the hard constraints of the controller), where the steepness is controlled by the weights and the controller horizon in Eq. 10.

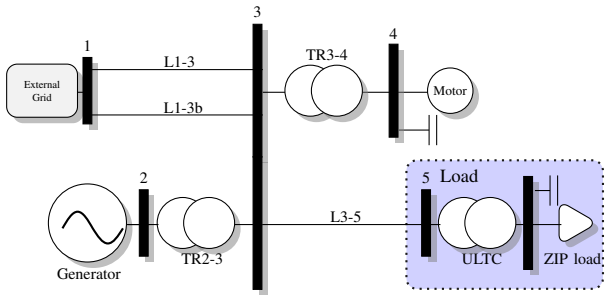

Fig. 4. Single line diagram of the single-machine test system.

TABLE I
ESTIMATED IMPROVED THERMAL-BASED OEL SYSTEM PARAMETERS OF THE TEST MACHINE BASED ON [13] AND [28].

Parameters	Description	Value (pu)
I_{fdn}	Rated Full Load Current (FLC)	1.71
I_{en}	OEL enabling current value	2.72
R_{rot}	Resistor of rotor winding	0.138
E_{cap}	Thermal capacity of the rotor	146

TABLE II
SINGLE MACHINE EVALUATION - COMPARISON OF METHODS

Method	Additional time	Relative improvement
Benchmark OEL	0 s	0 %
Improved OEL	151 s	46.5 %
Proposed ECD	325 s	100.0 %

IV. MULTI-MACHINE CASE SYSTEM

This section extends the single-machine case study in Section III with another case study, based on a larger multi-machine system. This is needed in order to fully demonstrate the advantages of the proposed ECD control system. Therefore, a dynamic study model has been developed based on the "Nordic Model High Load Case" from the Norwegian Transmission System Operator (TSO). The model setup and the simulations were done in the Matlab/Simulink environment. The geographical area under consideration is in the North region of Norway, containing four synchronous generators and one synchronous compensator. To fully address the aims of this paper, the model was tuned to operate near its capacity limit. In this adoption, cascading failures would inevitably lead to blackouts. The power system model is shown in Fig. 6.

A. External reactance sensitivity

The prediction of the UKF depends strongly on the precision of its underlying dynamic mathematical model. Therefore, the variation and sensitivity of the external grid reactance x_e was analyzed in detail. In fact, the short circuit power at the generator bus terminals in AREA 2 varies annually between 5 and 15 kA. The grid behaves weaker when the short-circuit capacity is small, i.e., large x_e in high-load case. In addition, the external grid equivalent will vary significantly during faulty conditions. Considering that there are no measurements available from the power system (emulated as Fig. 6), the model must be estimated based on the measurements carried

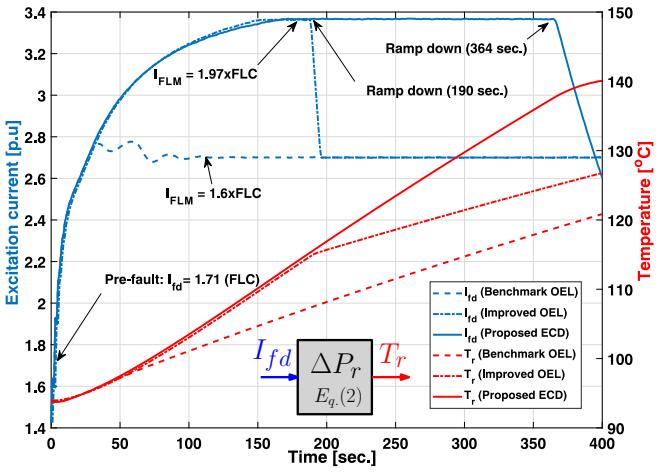

Fig. 5. Excitation current profiles for the benchmark OEL, improved thermal-based, and the proposed system with summation type control. The MISO controller horizon ($N_p = 10$ and $\Delta t = 2$ s) was 20 s. The field limiting model (FLM) and the start of ramp down are indicated in the figure.

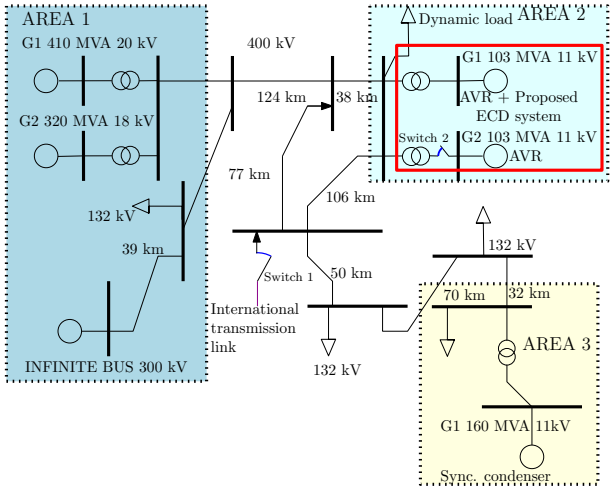

Fig. 6. Power system simulator for long term voltage stability simulations based on the Nordic Model from the Norwegian TSO. The system consists of three different areas including four synchronous generators and one synchronous condenser. Power is also fed through the international transmission link.

out at the generator terminals. As described in Section II-C, the external voltage V_e estimation is initially driven by white noise in the UKF, and the external reactance x_e is provided from SCA analysis. However, the UKF could be provided with an additional PMU measurement from the simulator (i.e., the real system). In this configuration, the external equivalent could be identified even after severe faults. This is visualized in Fig. 7. Because the proposed system works as a supervisory control system, an adjustment in the reactance yields little impact on the thermal state of the generator ($1-2°$C variation). The expected oscillating behaviour in the UKF may be different than the real system due to the sensitivity of x_e. However, this issue would be more severe if the NMPC would be operating as a primary controller.

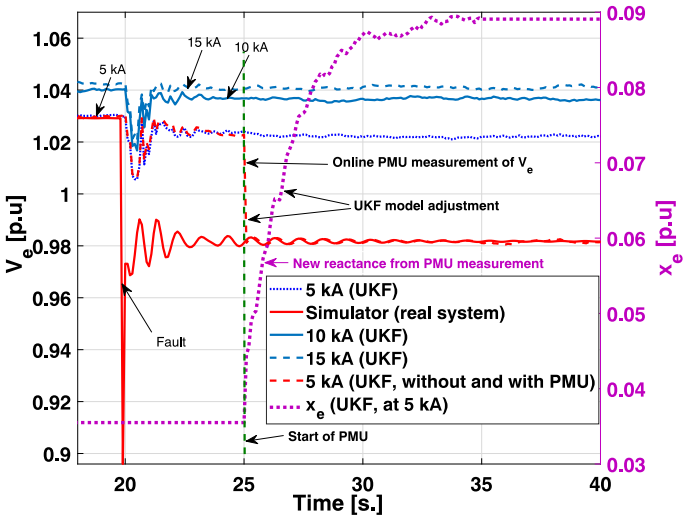

Fig. 7. Sensitivity in the voltage variation V_e of the external equivalent as the external reactance x_e of typical short circuit levels of 5, 10 and 15 kA are implemented in the UKF. In addition, the x_e can be identified through upstream PMU measurments (or any relevant position in the grid). The fault at 20 s. is the same as in subsection IV-B.

B. Contingency analysis

Contingency analysis is implemented in the large-scale system (Fig. 6). In particular, the N-1 contingency corresponds to a line outage. The proposed ECD control system is implemented at generator G1 in AREA 2. The objective is to reveal the overall performance of the multi-machine system. Studies are performed for single and multiple contingency cases to show the features of the proposed system comprehensively. In addition, the study explores the systems' ability to retain normal operating conditions after a fault clearing. The proposed system is implemented either as MISO and MIMO controller in the test cases (with $N_p = 20$, $N_c = 2$ and $\Delta t = 10$ s). The following assumptions are made for the case study of the Nordic power system:

- All hydrogenerators run initially at 0.85 p.u of nominal electrical power output.
- Cold coolant is assumed to be $20°\mathrm{C}$ in all the simulations, which realize a limiting observable temperature rise of $105°\mathrm{C}$ for the stator windings and $100°\mathrm{C}$ for the rotor windings [6] (e.g., $120°\mathrm{C}$ in figures).
- The benchmark models of the IEEE stator current limiter SC1L, and OELs with integral control of field current are initially implemented.
- The supervisory control signal is implemented as a summation type control to the AVR and governor.
- Generators in AREA 1 have the ST1A static excitation system implemented but no governor.

G1 in AREA 2 is where the proposed ECD system is implemented. The following conditions applies for AREA 2.

- The hydrogenerators are highly overexcited.
- G1 and G2 both have the ST1A excitation models and hydraulic turbine and governor models.
- The ratio on the primary side of the step-up transformers are adjusted to 0.9 p.u, and generators use a 50% reactive droop compensation of the transformer reactance.

Case 1 - Single contingency: This case considers an outage in the international transmission line at $t = 20\,\mathrm{s}$ (switch 1 in Fig. 6). After the disturbance, the generators in AREA 2 immediately supplies the reactive power demand of the system by increasing their excitation level, as shown in Fig. 8. Initially, the power system is equipped with the benchmark IEEE OEL and SC1L systems as seen in subcase 1A. The limitation of OEL starts almost instantly, according to the inverse-time characteristic. In this machine protection scheme, the SCL continues to reduce the field current after additional 20s. In the next sub cases, the conventional limiters are removed from generator G1 in AREA 2, and the proposed ECD system is implemented as a MISO control system. In subcase 1B, there are no constraints on the reactive power supply (no use of V_s), i.e., the temperature restriction of $120°\mathrm{C}$ are broken after $260\,\mathrm{s}$ (as seen in Fig. 8). In subcase 1C, a fast and large reduction of V_s provides loss of synchronization of the machine. Finally, in subcase 1D, the proposed control system has an additional constraint on the control input to prevent the previous scenario. In this setup, the constraints are broken after about $550\,\mathrm{s}$. The benchmark OEL systems are activated based on the level of voltage drop at the generator terminals (e.g, as a consequence of the electrical distance from the location of the event), while the proposed ECD system is activated based on the online thermal capacity of the generator in addition to its electrical distance from the disturbance incident.

In continuation of this, the proposed control system is implemented as a MIMO system, i.e., controlling both the excitation V_s and the power P_{m_0}. A reduction of one or both of these inputs consequently reduces the field current I_{fd} and the terminal current I_t of the controlled machine (A2.G1). As seen in Fig. 9, the time for the enhanced operation is now extended to above $730\,\mathrm{s}$ as the active power is ramped down $0.2\,\mathrm{p\,u}$ after a maximum reduction of the field current. In addition, the corresponding changes in the field current level of the different generators in the 16-bus multi-machine system are also plotted. The different machines contribute based on their distance from the location of the event.

Case 2 - Multiple contingency: The contingency considered in this case is the outage of the same line as above at $t = 20\,\mathrm{s}$ (switch 1 in Fig. 6). In addition, an outage of G2 in AREA 2 at $t = 50\,\mathrm{s}$ (switch 2 in Fig. 6) occurs. The excitation level of the generator G1 following the disturbances is presented in Fig. 10. The excitation system of the G1 machine is now heavily loaded, and it quickly reaches its limits. However, due to the thermal flexibility of the controller, the injection of reactive power continues until $160\,\mathrm{s}$ before the controller initiates reduction of the excitation current (MISO). Moreover, the turbine power starts to ramp down at $175\,\mathrm{s}$ (MIMO). The supervisory system is not allowed to increase the set-point defined by the operator during this stage. However, the line is reconnected after $220\,\mathrm{s}$ and the NMPC steers the system back to its references. As long as the temperature constraints are not broken in the horizon of the supervisory controller, the

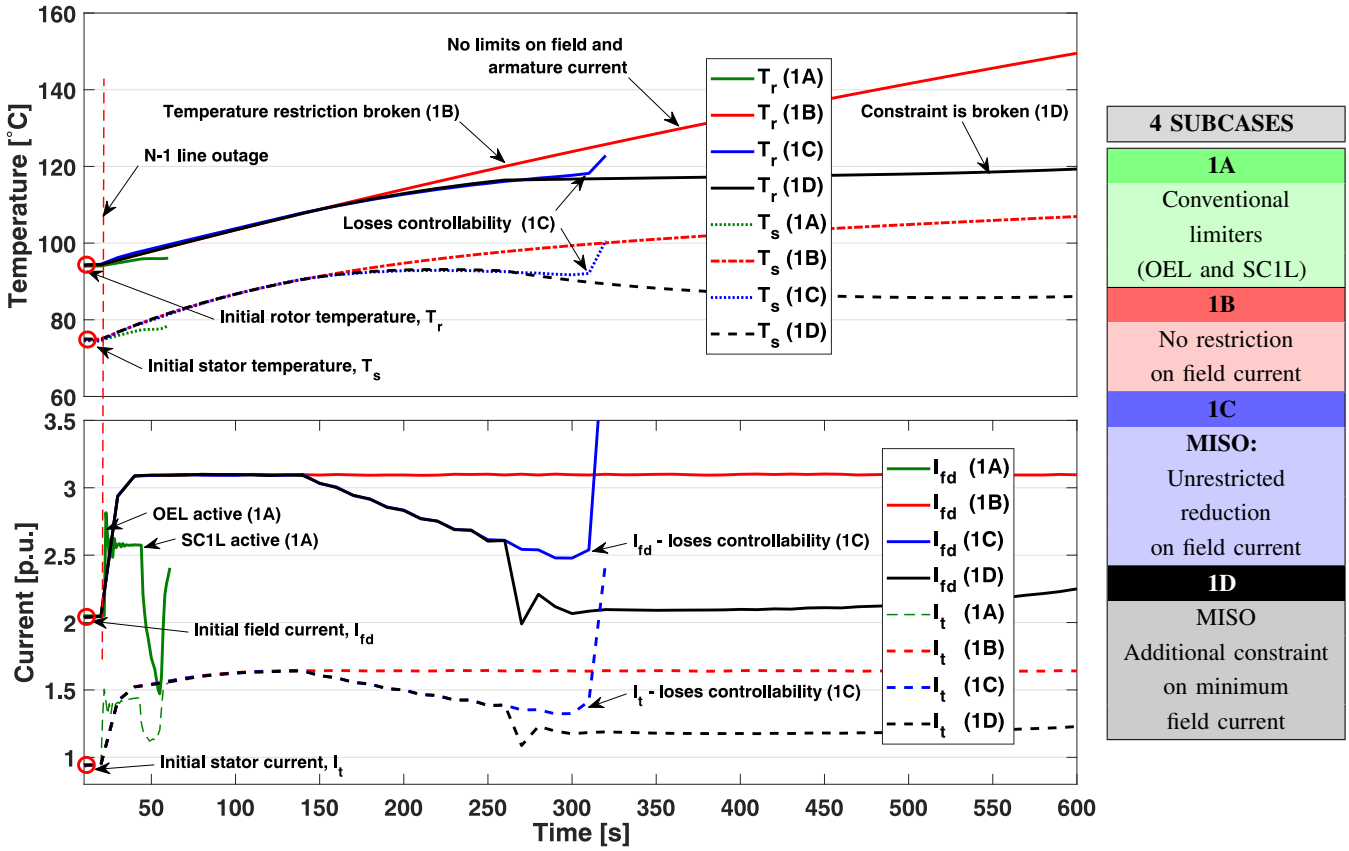

Fig. 8. Four different simulations (subcases) under the influence of the same single contingency. The subcase 1C and 1D are with MISO controller performance of the proposed ECD system (at G1 in AREA 2)

AVR will again regulate the voltage freely at the generator terminals.

V. Discussion

In this paper, it has been shown that the online proposed system exhibits a significant increase in the activation time of

- 174 s in comparison to the thermal-based improved OEL system [13], and
- 325 s in comparison to the benchmark OEL system.

Using the single-machine test system, the simulation results show that the proposed method can efficiently utilize the thermal capacity of the rotor and inject more reactive power into the system and surpasses earlier proposed systems.

The performance of the proposed ECD method is further validated in a case study based on the Nordic model from the Norwegian TSO. The system demonstrates its effectiveness in extending the amount of reactive power that can be supplied into a multi-machine network, resulting in an improved voltage stability of the system. Due to the large thermal time constants of the machine, the proposed control system exhibits a maximum time of 550 s (Fig. 8) with MISO control system and beyond 730 s (Fig. 9) with MIMO system control. In fact, ECD operation beyond 730 s in MIMO mode is constrained by the limitations in allowed turbine power reduction (maximum reduction P_e from 0.85 pu to 0.65 pu in this case study). This is because the MIMO control structure reduces the active power through the governor to increase the ability for reactive power support. Simulations (Fig. 9) shows that the MIMO functionality works on a component level. However, the frequency restoration requirements demands that a reduction of the active power can only be permitted as long as other distributed generator units complement with an increase in their active power production. Further work on the active power coordination in the ECD scheme with rescheduling of the active power dispatch between multiple generators during a contingency should be investigated. In addition, the minimization of the grid losses depending on the location of the generator would be a future research item. However, this paper already demonstrates the promising ability of the proposed ECD control system to further extend the under-voltage ride-through time. As a result, it emerges as an important measure to avert a blackout of the power system. Finally, the maximum reactive power utilization of the machine is achieved.

As evident in this paper, there is extensive thermal capacity available both in the rotor and the stator of synchronous generators. Considering the proposed flexibility, the machine may deliver more active power as well, in combination with a sufficient amount of reactive power. The lifetime for a synchronous machine is considered to be much longer than the turbine. Therefore, it is an inevitable fact that the turbines have to be replaced. Considering the flexibility of the proposed system, the operator is given the opportunity to upgrade the size of the turbine, as indicated in Fig. 1. Hence, a flexible

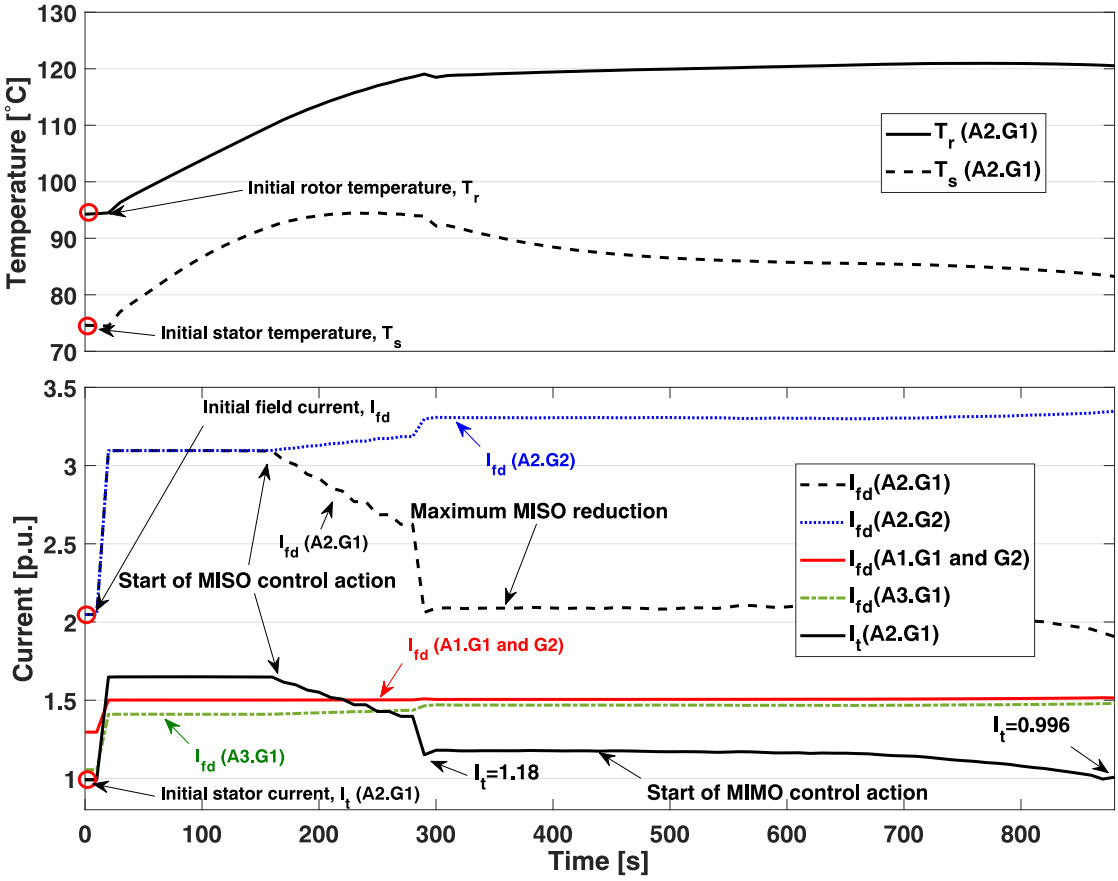

Fig. 9. MIMO controller performance of the proposed ECD system (at G1 in AREA 2) during a single contingency.

power factor redesign may be employed with the proposed method. Among the restrictions are the insulation standards of the materials in the machine. Considering that class F exhibits a maximum temperature of 155°C, extended time could be provided depending on the cold coolant temperature, hot-spot temperatures, and how the machine is subjected to frequent cyclic loading. In this realm of opportunities, more constraints need to be considered in the controller to ensure the desired control performance. The proposed system should employ hot-spot considerations. The ratio between hot-spot and the observable sensor temperature identified through FEM analysis should be implemented as a safety margin for the controller [28]. In addition, the reduction of field current during a disturbance should be made with great care as it can exhibit instability and loss of synchronism.

In brief, this paper demonstrates the applicability of transforming the generator's thermal reserve into an applicable amount of reactive power reserve capacity. Note that an extensive use of the ECD will not frequently occur to the specific generator. Limited use of the ECD scheme reduces the impact of long-term thermal stress effects. In fact, utilizing the ECD method is shown to be an efficient exploitation of the machine to secure the power system reliability. As a result, it may prove its effectiveness as a security indicator, such as the amount of spinning MW reserve does. If incentives are provided through the provision of emergency control services in the electric power market [13], the generator owners may be more convinced to utilize the available reactive power of their generators to improve power system performance and voltage stability. Moreover, a reduction in the investment cost of power electronics in compensating devices on the grid side would further justify the implementation of the ECD method.

A current challenge for the ECD method includes a higher level of excitation current capability required by the thyristors (static exciter). However, cyclic overloading of thyristors is possible because they are typically over-rated [32]. To further improve the system security, temperature monitoring of thyristors, transformers, and supplying power cables would be an advantage when the machine is operated in extreme modes of over-excitation. However, the under-voltage scenario causes the generator stator to be less effected by saturation phenomena [28], which simplifies the electrical modeling.

In this paper, the ECD method is applied to a hydrogenerator. However, the scheme can in principle be used to extend the capability of any air-cooled generator. As a result, it can be employed in multi-site installations as well. Recently, excitation boosters for short-term fault-ride through capability enhancement has already shown promising results [33].

Finally, to be able to utilize the system in reality, NMPC would require extensive computing power to solve non-linear constrained optimization problems in real time. However, due to the large thermal time constants in the machine and the

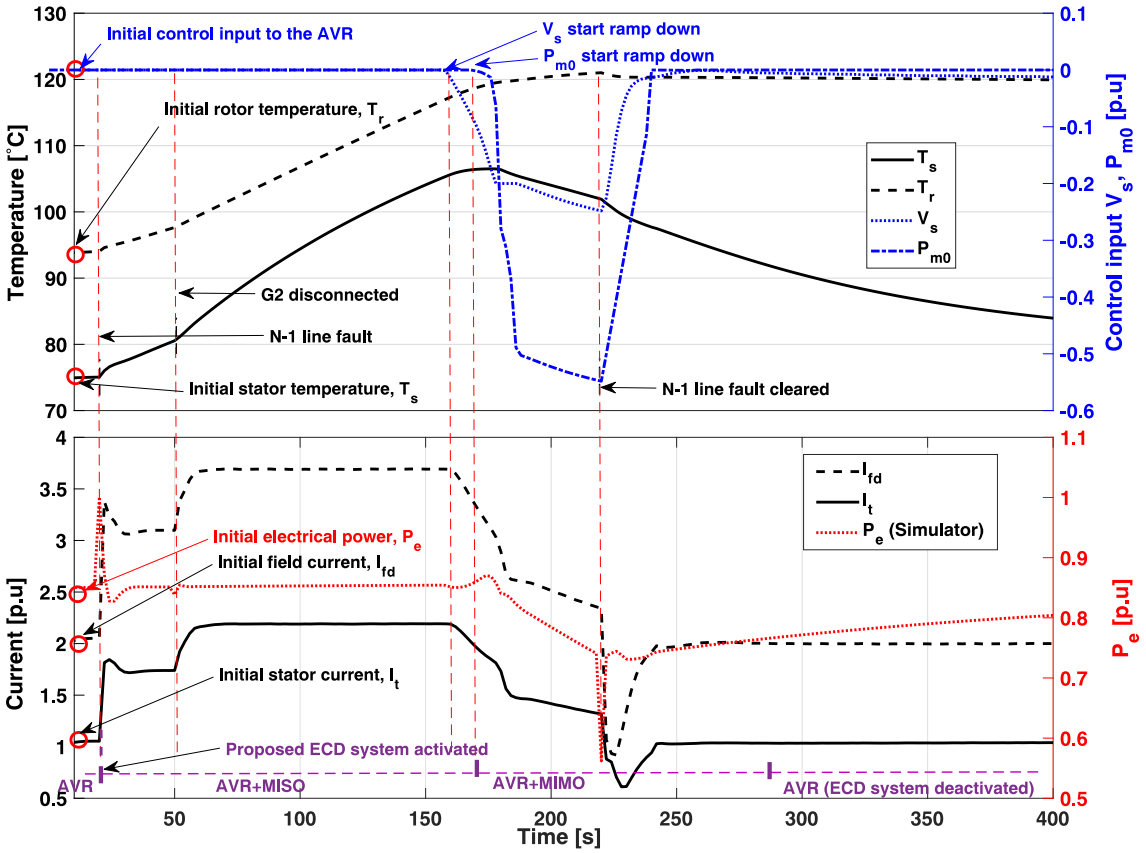

Fig. 10. Multiple contingency considerations with line outage at $t = 20\,\text{s}$ and G2 outage at $t = 50\,\text{s}$. The line is reconnected at $t = 220\,\text{s}$. An activation time-line of the control structure is indicated in the figure.

typical time period for long term voltage stability, the proposed method holds real-time opportunities.

VI. Conclusion

A new supervisory model-based control system for generator units is proposed. The controller utilizes an Enhanced Capability Diagram (ECD) that are established from a thermal model. It is shown to be more effective than existing methods. In particular, the system is able to do the following.

- Track any desired set-point value and retain any physical constraint specified by the operator;
- Extend the activation time compared with existing reactive power limiters (174 s extension);
- Enhance the voltage support under a disturbance, and provide the operators more time to determine the best countermeasure that can be effective mitigating the emergency condition;
- And realize a superior flexibility in active power production under normal operation.

The work is expected to guide operators in the implementation of more realistic activation times in conventional limiters. In the future, the scheme could be further improved by utilizing high-quality PMU data and new communication interfaces at the grid cite. Additionally, the development of a coordinated scheme for multi-cite installation in large scale applications will be further investigated.

References

[1] J.-H. Braam, "Development, test and validation of new generator product line for current and future operational regimes," *CIGRE*, 2018.

[2] N. Yorino, M. Abdillah, Y. Sasaki, and Y. Zoka, "Robust power system security assessment under uncertainties using bi-level optimization," *IEEE Trans. Power Syst.*, vol. 33, no. 1, pp. 352–362, Jan 2018.

[3] S. Paladhi and A. K. Pradhan, "Adaptive zone-1 setting following structural and operational changes in power system," *IEEE Trans. Power Delivery*, vol. 33, no. 2, pp. 560–569, April 2018.

[4] W. Qin, P. Wang, X. Han, and X. Du, "Reactive power aspects in reliability assessment of power systems," *IEEE Trans. Power Syst.*, vol. 26, no. 1, pp. 85–92, Feb 2011.

[5] M. Eremia and M. Shahidehpour, *Major Grid Blackouts: Analysis, Classification, and Prevention*. IEEE, 2013. [Online]. Available: https://ieeexplore.ieee.org/xpl/articleDetails.jsp?arnumber=6482751

[6] IEEE, "Standard for salient-pole 50 hz and 60 hz synchronous generators and generator/motors for hydraulic turbine applications rated 5 mva and above," *IEEE Std C50.12-2005*, pp. 1–45, Feb 2006.

[7] M. Guan, W. Pan, J. Zhang, Q. Hao, J. Cheng, and X. Zheng, "Synchronous generator emulation control strategy for voltage source converter (vsc) stations," *IEEE Trans. Power Syst.*, vol. 30, no. 6, pp. 3093–3101, Nov 2015.

[8] J. Renedo, A. García-Cerrada, and L. Rouco, "Reactive-power coordination in vsc-hvdc multi-terminal systems for transient stability improvement," *IEEE Trans. Power Syst.*, vol. 32, no. 5, pp. 3758–3767, Sep. 2017.

[9] S. D. Naik, S. S. Bhat, and M. K. Khedkar, "Effect of generator reactive power limit on proximity to voltage instability of multibus power system," in *Proc. 12th IEEE Conf. Ind. Electron. Appl. (ICIEA)*, June 2017, pp. 613–617.

[10] A. Murdoch, G. E. Boukarim, B. E. Gott, M. J. D'Antonio, and R. A. Lawson, "Generator over excitation capability and excitation system limiters," *Proc. IEEE PES Winter Meeting.*, pp. 215–220 vol.1, Jan. 2001.

[11] E. Pajuelo, R. Gokaraju, and M. S. Sachdev, "Coordination of overexcitation limiter, field overcurrent protection and generator control," in *Proc. IEEE PES Gen. Meeting*, July 2010, pp. 1–7.

[12] R. Kutzner, M. Lösing, U. Seeger, and A. Wenzel, "Application of stator current limiter: Impact during system voltage decrease," in *Proc. IEEE PES Gen. Meeting*, July 2013, pp. 1–5.

[13] H. Lomei, K. M. Muttaqi, and D. Sutanto, "A new method to determine the activation time of the overexcitation limiter based on available generator rotor thermal capacity for improving long-term voltage instability," *IEEE Trans. Power Syst.*, vol. 32, no. 3, pp. 1711–1720, May 2017.

[14] B. Gong and I. Hiskens, "A stable finite horizon model predictive control for power system voltage collapse prevention," in *Proc. 50th IEEE Conf. on Decision Contr., European Contr. Conf.*, Dec 2011, pp. 7105–7110.

[15] B. Otomega, A. Marinakis, M. Glavic, and T. V. Cutsem, "Model predictive control to alleviate thermal overloads," *IEEE Trans. Power Syst.*, vol. 22, no. 3, pp. 1384–1385, Aug 2007.

[16] A. N. Venkat, I. A. Hiskens, J. B. Rawlings, and S. J. Wright, "Distributed mpc strategies with application to power system automatic generation control," *IEEE Trans. Control Syst. Technol.*, vol. 16, no. 6, pp. 1192–1206, Nov 2008.

[17] J. A. Martin and I. A. Hiskens, "Corrective model-predictive control in large electric power systems," *IEEE Trans. Pow. Syst.*, vol. 32, no. 2, pp. 1651–1662, March 2017.

[18] T. Sun, J. Wang, A. Griffo, and B. Sen, "Active thermal management for interior permanent magnet synchronous machine (ipmsm) drives based on model predictive control," *IEEE Trans. Ind. Appl.*, pp. 1–1, 2018.

[19] Y. Liu, S. Cheng, B. Ning, and Y. Li, "Robust model predictive control with simplified repetitive control for electrical machine drives," *IEEE Trans. Power Electron.*, vol. 34, no. 5, pp. 4524–4535, May 2019.

[20] E. Kayacan, E. Kayacan, H. Ramon, and W. Saeys, "Learning in centralized nonlinear model predictive control: Application to an autonomous tractor-trailer system," *IEEE Trans. Control Syst. Techol.*, vol. 23, no. 1, pp. 197–205, Jan 2015.

[21] L. Samaranayake and S. Longo, "Degradation control for electric vehicle machines using nonlinear model predictive control," *IEEE Trans. Control Syst. Technol.*, vol. 26, no. 1, pp. 89–101, Jan 2018.

[22] E. Ghahremani and I. Kamwa, "Online state estimation of a synchronous generator using unscented kalman filter from phasor measurements units," *IEEE Trans. Energy Convers.*, vol. 26, no. 4, pp. 1099–1108, Dec 2011.

[23] A. Rouhani and A. Abur, "Constrained iterated unscented kalman filter for dynamic state and parameter estimation," *IEEE Trans. Power Syst.*, vol. 33, no. 3, pp. 2404–2414, May 2018.

[24] N. Zhou, D. Meng, and S. Lu, "Estimation of the dynamic states of synchronous machines using an extended particle filter," *IEEE Trans. Power Syst.*, vol. 28, no. 4, pp. 4152–4161, Nov 2013.

[25] A. Rouhani and A. Abur, "Observability analysis for dynamic state estimation of synchronous machines," *IEEE Trans. Power Syst.*, vol. 32, no. 4, pp. 3168–3175, July 2017.

[26] H. M. T. Menegaz, J. Y. Ishihara, G. A. Borges, and A. N. Vargas, "A systematization of the unscented kalman filter theory," *IEEE Trans. Autom. Control*, vol. 60, no. 10, pp. 2583–2598, Oct 2015.

[27] D. Simon, *Optimal State Estimation: Kalman, H Infinity, and Nonlinear Approaches*. Wiley-Interscience, 2006.

[28] T. Øyvang, J. K. Nøland, G. J. Hegglid, and B. Lie, "Online model-based thermal prediction for flexible control of an air-cooled hydrogenerator," *IEEE Trans. Ind. Electron.*, vol. 66, no. 8, pp. 6311–6320, Aug 2019.

[29] H. Gharavi and B. Hu, "Synchrophasor sensor networks for grid communication and protection," *Proc. IEEE*, vol. 105, no. 7, pp. 1408–1428, Jul. 2017.

[30] T. Øyvang, G. J. Hegglid, and B. Lie, "Models of synchronous generators with excitation system, for transient power system studies," *IFAC-PapersOnLine*, vol. 51, no. 2, pp. 91 – 96, 2018, proc. 9th Vienna Int. Conf. Math. Modelling.

[31] W. R. Lachs and D. Sutanto, "Rotor heating as an indicator of system voltage instability," *IEEE Trans. Power Syst.*, vol. 10, no. 1, pp. 175–181, Feb 1995.

[32] W. D. Walker and W. F. Weldon, "Thermal modeling and experimentation to determine maximum power capability of scr's and thyristors," *IEEE Trans. Ind. Electron.*, vol. 14, no. 2, pp. 316–322, March 1999.

[33] L. Díez-Maroto, J. Renedo, L. Rouco, and F. Fernández-Bernal, "Lyapunov stability based wide area control systems for excitation boosters in synchronous generators," *IEEE Trans. Power Syst.*, vol. 34, no. 1, pp. 194–204, Jan 2019.

Thomas Øyvang (S'17–M'19) received the Ph.D. degree in Process, Energy and Automation from the University of South–Eastern Norway (USN) in 2018. Since January 2019 he has been an Associate Professor, and the R&D manager for the research group Hydro Power, Transmission and Distribution with the USN, Porsgrunn. His research interests include control systems, salient-pole synchronous generators, and power system dynamics. Dr. Øyvang is a Board Member of the Norwegian Academic Committee of Publication in Technology.

Jonas Kristiansen Nøland (S'14–M'17) received the Ph.D. degree in engineering physics from Uppsala University, Uppsala, Sweden, in 2017. In April 2017, he became an Associate Professor with the University of South-Eastern Norway, Porsgrunn, Norway. From December 2018, he has been an Associate Professor with the Department of Electric Power Engineering, Norwegian University of Science and Technology, Trondheim, Norway. His research interests include excitation systems, salient-pole synchronous generators, and their interplay with the power system. Dr. Nøland currently serves as an Editor within power generation subject areas for the IEEE TRANSACTIONS ON ENERGY CONVERSION. He is a Board Member of the Norwegian Academic Committee of Publication in Technology. He is also on the Steering Committee of the IEEE Power and Energy Chapter of Norway.

Roshan Sharma is an Associate Professor at the University of South–Eastern Norway, Norway. He received a Ph.D. degree in Process, Energy and Automation from Telemark University College in 2014. His areas of expertise are model based advanced control, process optimization, and state and parameter estimation. He has been actively working as a researcher within the energy related industries since 2011.

Gunne J. Hegglid received his Ph.D. degree in Multivariable control scheme for hydropower units from Norwegian University of Science (NTNU), Norway, in 1981. Between 81 and 82 he was a researcher at Sintef, Trondheim, Norway. In 1982 until 1998 he worked with the Consulting group IGP AS in Trondheim (now Cowi) as Senior engineer. In 1998, he joined SKK AS (now Skagerak Energi AS) in Porsgrunn as chief engineer. In 2015, he joined USN as Professor II in Electrical engineering.

Bernt Lie (M'97) received his Ph.D. degree in Engineering Cybernetics from Norwegian University of Science and Technology (NTNU), Norway, in 1990. From 1987-1991 he was assistant and associate professor at NTNU. In 1992, he joined University of South-Eastern Norway, where he is currently Professor of Informatics and leads the Telemark Modeling and Control Center. His research focuses on control relevant modeling and advanced control, with applications mainly within the process and energy industries.